eLIFE elifesciences.org

RESEARCH ARTICLE

Figures and figure supplements

C-mannosylation supports folding and enhances stability of thrombospondin repeats

Aleksandra Shcherbakova *et al*

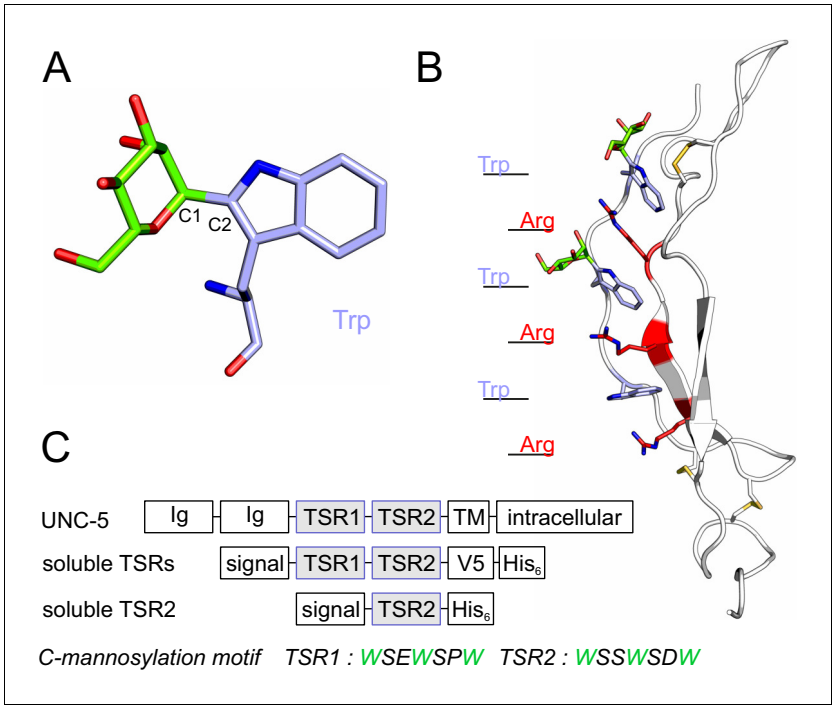

Figure 1. C-mannosylation of thrombospondin type 1 repeats. (**A**) C-mannose (green) linked to the indole C2 atom of a tryptophan (light-blue) by a C-C bond. (**B**) Modeled structure of *C. elegans* UNC-5 TSR2 with tryptophans (blue) and arginines (red) arranged in a Trp-Arg ladder. C-mannoses (green) are displayed on the first two tryptophans of the WXXWXXW motif, according to previous findings (***Buettner et al., 2013***), (***Figure 3—figure supplement 1***). Oxygen atoms are indicated in red, nitrogen atoms in dark-blue and disulfide bonds in yellow. (**C**) Natural *C. elegans* UNC-5 and soluble TSR constructs applied in this study. Ig: immunoglobulin-like domain; TSR: thrombospondin type 1 repeat; TM: transmembrane domain; signal: cleavable secretion signal; V5 and His_6: tags for detection and purification.

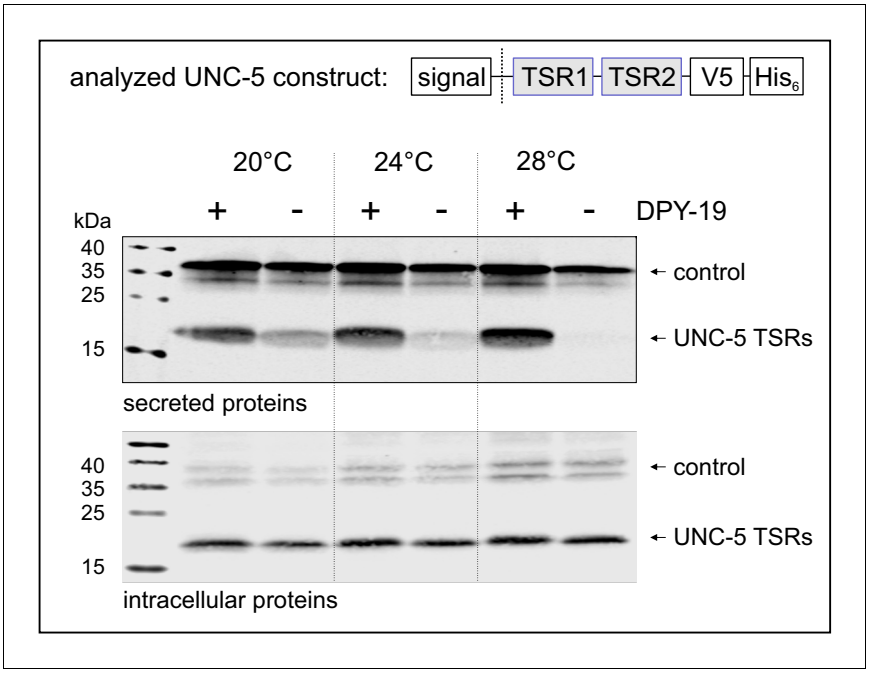

Figure 2. Effects of C-mannosylation on TSR secretion. Western blot analysis of secreted (upper panel) and intracellular (lower panel) UNC-5 TSRs 1+2 expressed in *Drosophila* S2 cells, co-transfected with *C. elegans* DPY-19 (+) or an empty vector (-) and incubated at 20, 24°C and 28°C as indicated. V5-tagged EGF repeats 16–20 from *Drosophila* Notch were used as transfection and secretion control. Both proteins were detected by anti-V5 antibody. An analog temperature-sensitivity can be observed in *C. elegans dpy-19* mutants (***Figure 2—figure supplement 1***).

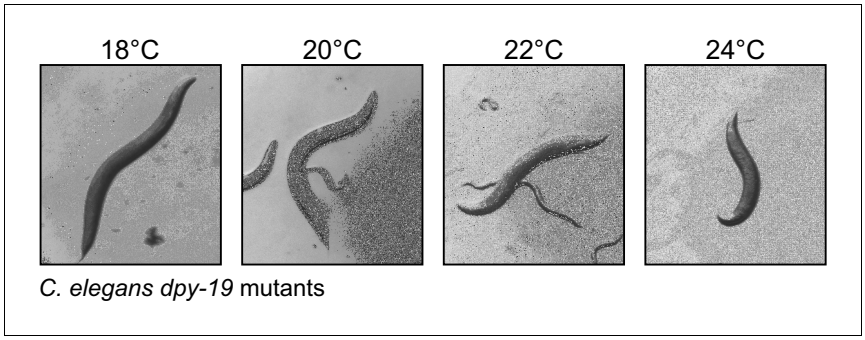

Figure 2—figure supplement 1. The temperature-sensitive dumpy phenotype of *C. elegans dpy-19* mutants. *C. elegans dpy-19*(e1259)III worms (strain CB1259 from the *Caenorhabditis* Genetics Center) were grown on *E. coli* OP50 cells as described in WormBook (www.wormbook.org) at 18, 20, 22 and 24˚C.

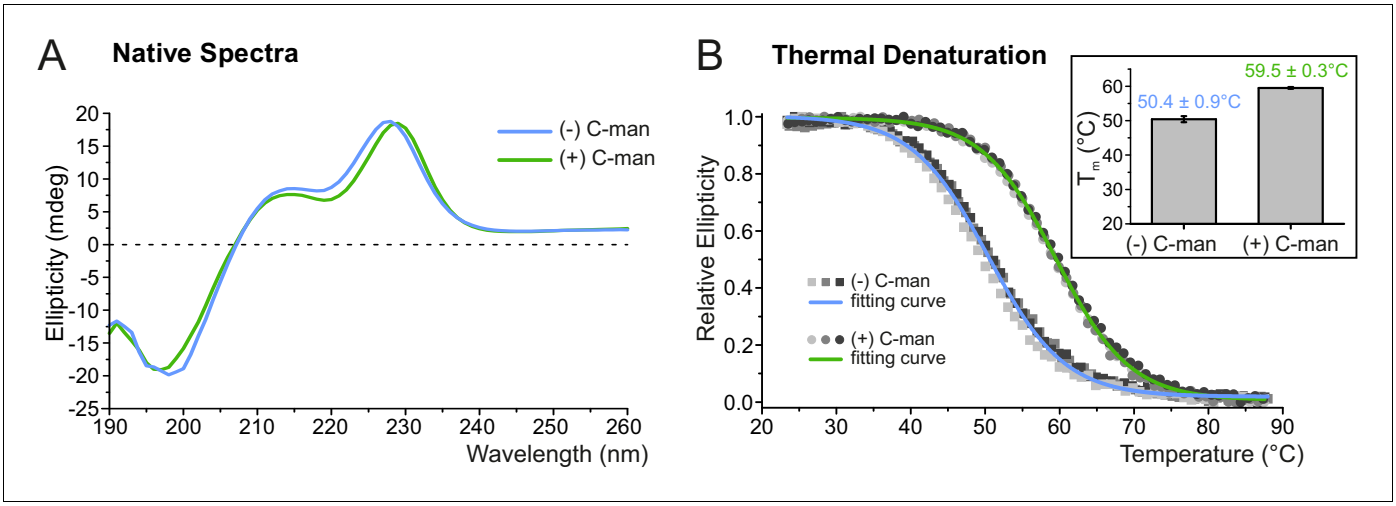

Figure 3. C-mannosylation increases resistance of UNC-5 TSR2 to thermal denaturation. (**A**) Native CD spectra of non-mannosylated (blue) and C-mannosylated (green) UNC-5 TSR2 at 24˚C. Average spectra of three measurements are displayed for each TSR form (***Figure 3—source data 1***). (**B**) Thermal denaturation of non- and C-mannosylated UNC-5 TSR2 monitored by CD spectroscopy at a wavelength of 229 and 228 nm, respectively. Measurements of three non-mannosylated (gray-shaded squares) and C-mannosylated (gray-shaded circles) UNC-5 TSR2 samples were averaged and fitted (blue and green, respectively) (***Figure 3—source data 2***). Average T_m values are depicted in the right plot (error bars show standard deviation). Thermal denaturation of both, non- and C-mannosylated TSRs, was reversible to a high extent (***Figure 3—figure supplement 2***).

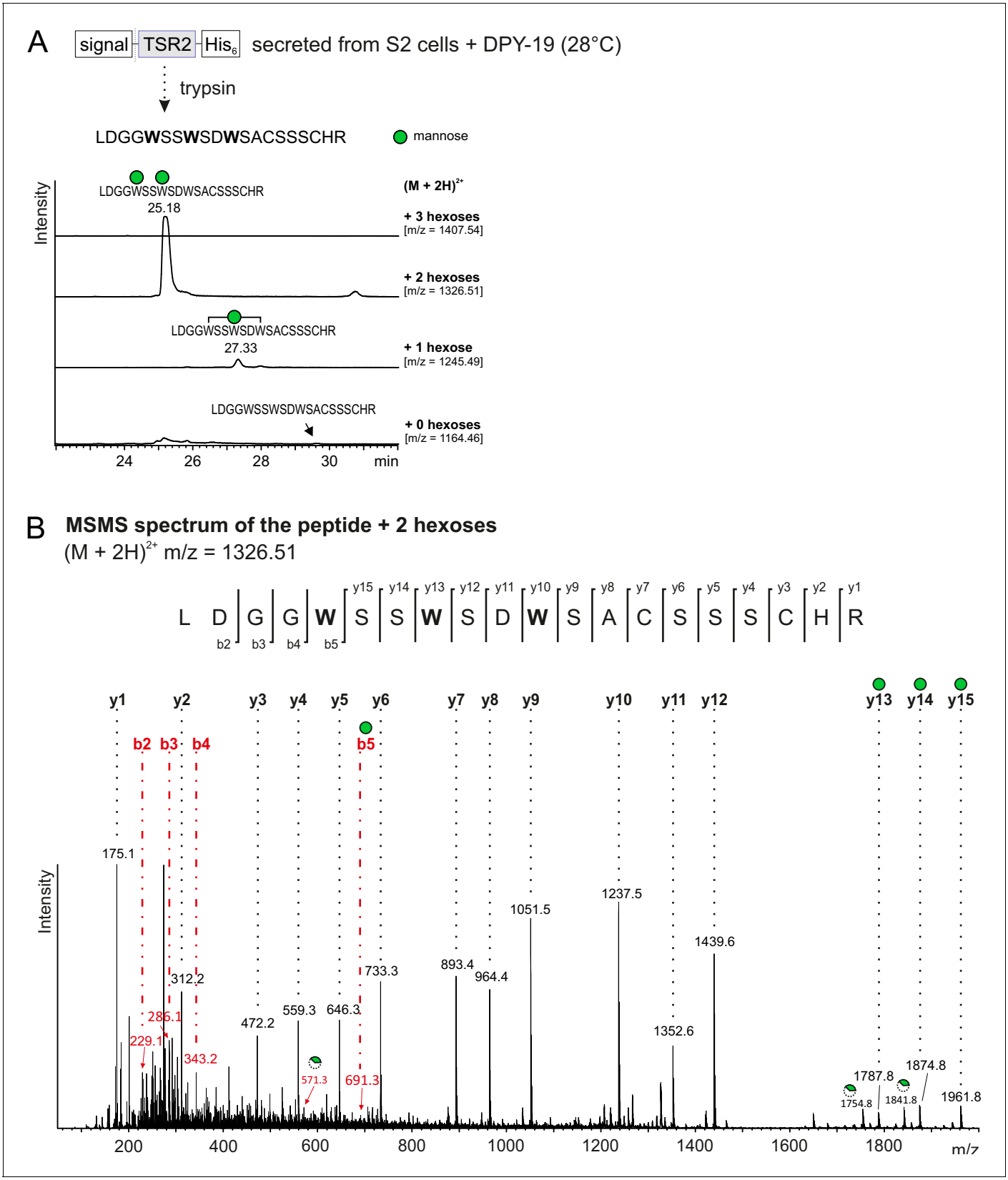

Figure 3—figure supplement 1. Mass spectrometry analysis of UNC-5 TSR2 co-expressed with DPY-19. (**A**) Extracted ion chromatograms of $(M + 2H)^{2+}$ ions of the UNC-5 TSR2 tryptic peptide containing the WXXWXXW motif with no, one, two and three hexoses are displayed revealing that the di-

Figure 3—figure supplement 1 continued on next page

Figure 3—figure supplement 1 continued

mannosylated form is most abundant. (**B**) MSMS spectrum of the di-mannosylated UNC-5 TSR2 (m/z = 1326.51) showing that the two C-mannoses are located on the first two tryptophans of the WXXWXXW motif. b- and y- series ions with additional hexose masses are marked either by a green circle displaying a full mannose or by a broken circle displaying a cross-ring cleaved C-mannose (loss of 120 Da).

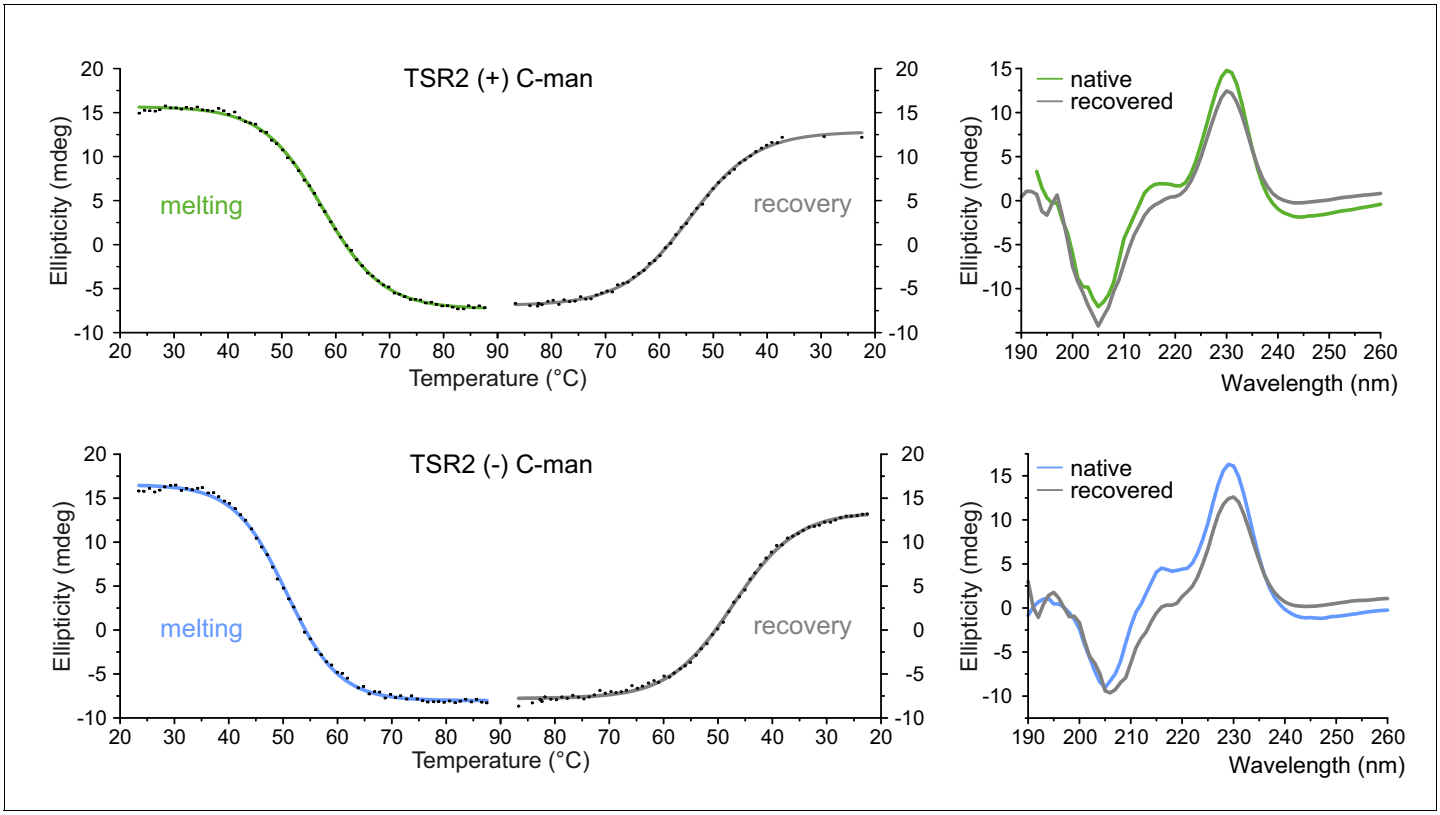

Figure 3—figure supplement 2. Recovery of thermally denatured UNC-5 TSR2 with and without C-mannosylation. Thermal denaturation and recovery upon temperature decrease of C-mannosylated (green) and non-mannosylated (blue) UNC-5 TSR2 were monitored by CD spectroscopy at a wavelength of 228 and 229 nm, respectively. Collected data points were fitted by Boltzmann function (OriginLab). 260–190 nm spectra of native and recovered TSRs display refolding of the proteins to a high extent.

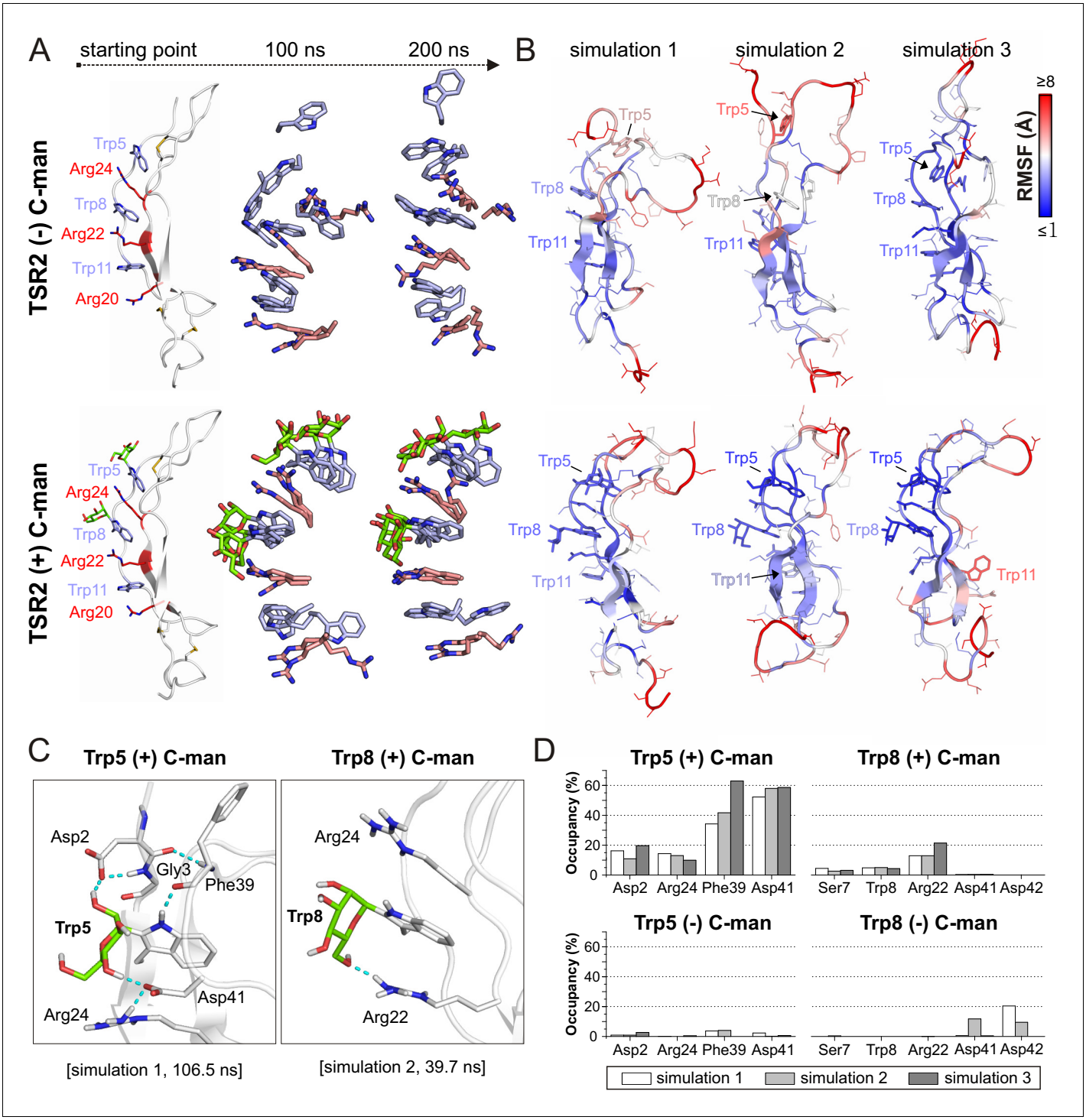

Figure 4. Molecular dynamics simulations at elevated temperature. (**A**) Modeled structures of UNC-5 TSR2 without C-mannosylation (top) and with two C-mannoses on Trp5 and Trp8 (bottom) at the starting point of each simulation followed by aligned Trp-Arg ladder structures from three simulation replicates after 100 and 200 ns simulation time. Tryptophans are depicted in light-blue, mannoses in green and arginines in salmon. (**B**) Representative most-abundant structures of non- and C-mannosylated UNC-5 TSR2 from each simulation, colored using a blue-white-red gradient according to the calculated root-mean-square fluctuation (RMSF) values (blue ≤1 Å; red ≥8 Å) (***Figure 4—figure supplement 1***, ***Figure 4—source data 1***). (**C**) Hydrogen bonds (cyan) formed by C-mannosylated Trp5 and Trp8 with adjacent residues, calculated using the VMD Hydrogen Bonds plugin. Oxygen atoms are depicted in red and nitrogen atoms in dark-blue. (**D**) Most abundant hydrogen bonds formed during each simulation either by C-mannoses together with corresponding tryptophan residues or by non-mannosylated tryptophans alone are displayed as occupancies (%). A more detailed representation is depicted in ***Figure 4—figure supplement 4***.

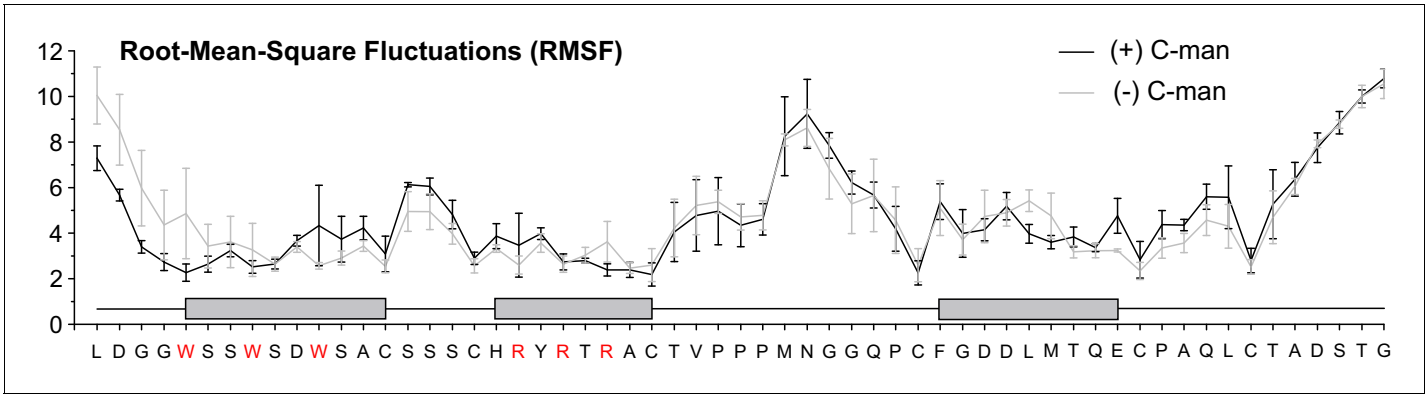

Figure 4—figure supplement 1. Side chain Root-Mean-Square Fluctuations (RMSF) of all residues from molecular dynamics simulations at elevated temperature. Mean RMSF values from simulation triplicates are shown in black for the C-mannosylated and in gray for the non-mannosylated TSR. Error bars depict calculated standard error. The three TSR beta-strands are displayed as gray boxes above the protein sequence. Tryptophan and arginine residues forming the Trp-Arg ladder are highlighted in red.

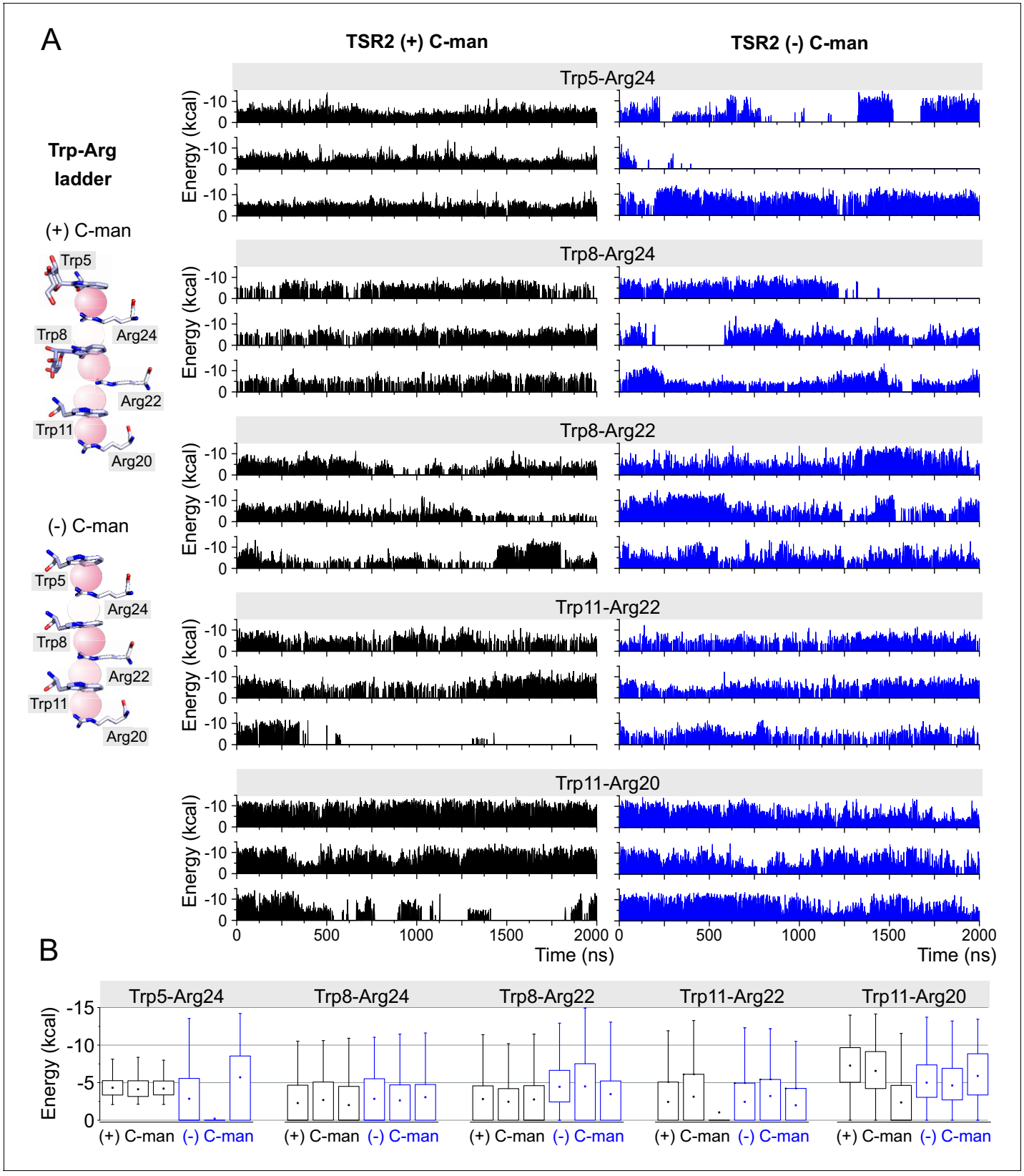

Figure 4—figure supplement 2. Cation-π interactions between Trp and Arg residues in the Trp-Arg ladder of the C-mannosylated (black) and non-mannosylated (blue) UNC-5 TSR2 during molecular dynamics simulation at elevated temperature. (**A**) The energies were calculated using the CaPTURE program (***Gallivan and Dougherty, 1999***) and are displayed for each interacting Trp and Arg residue pair in each simulation triplicate. (**B**)

Figure 4—figure supplement 2 continued on next page

Figure 4—figure supplement 2 continued

Representation of the energy values as mean values for each residue pair with corresponding interquartile (boxes) and 5th/95th percentile (whiskers) ranges.

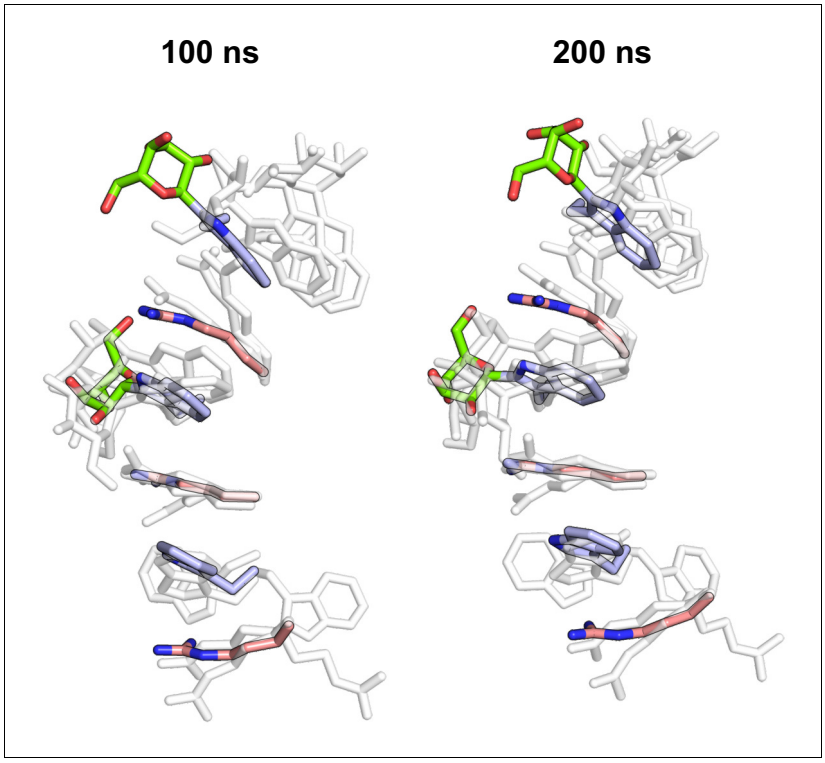

Figure 4—figure supplement 3. Molecular dynamics simulations of C-mannosylated UNC-5 TSR2 at elevated temperature with C-mannoses in the $^{1}C_{4}$ conformation. Trp-Arg ladder after 100 and 200 ns simulation time is displayed aligned with corresponding Trp-Arg ladder structures from UNC-5 TSR2 with $^{4}C_{1}$ C-mannoses (transparent). Tryptophans are depicted in light-blue, C-mannoses in green, arginines in salmon, oxygen atoms in red and nitrogen atoms in blue.

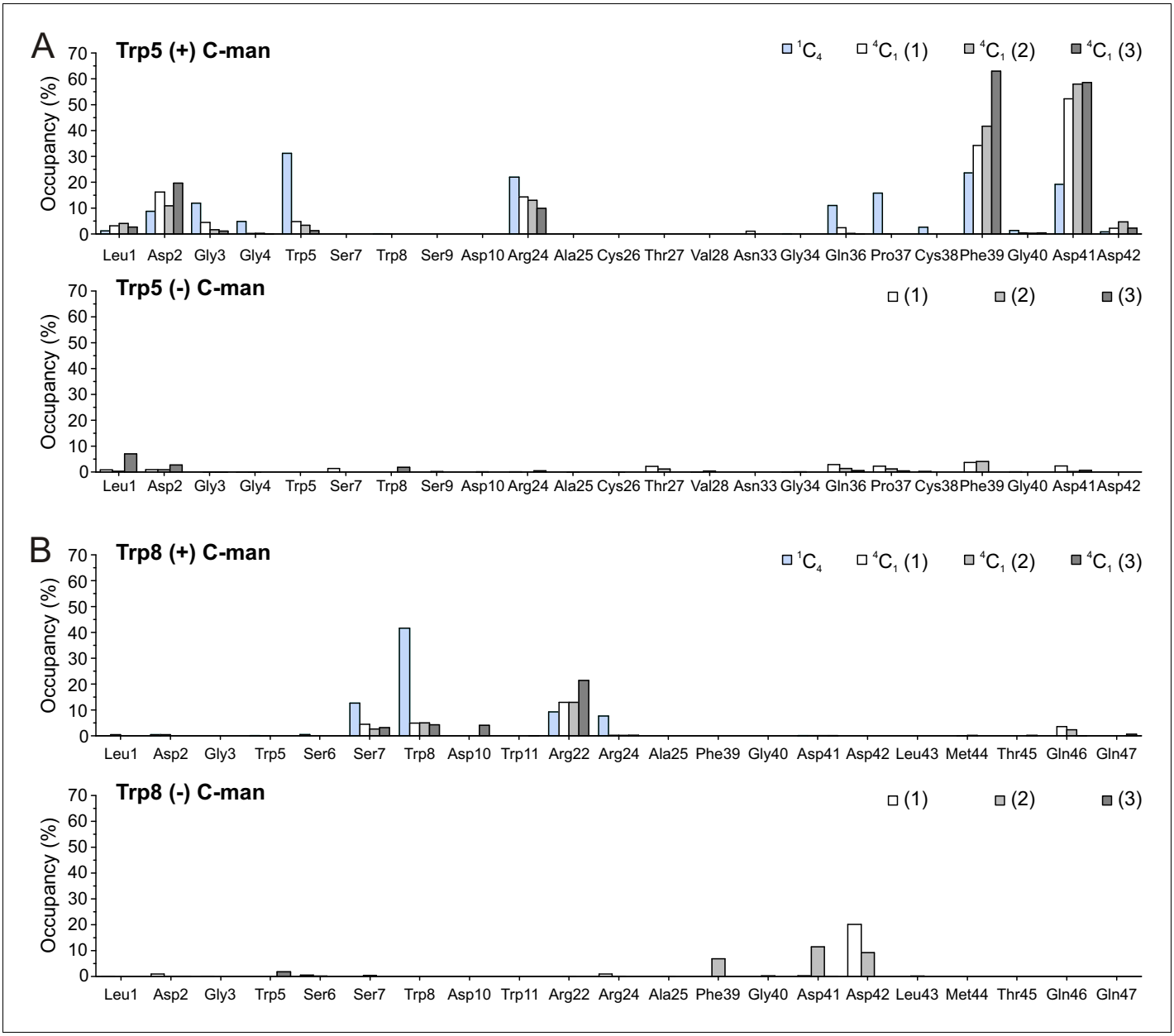

Figure 4—figure supplement 4. Total hydrogen bonds formed by C- and non-mannosylated Trp5 (**A**) and Trp8 (**B**) during molecular dynamics simulations at elevated temperature. Gray bars display hydrogen bonds from three independent simulations formed either by tryptophans with $^4C_1$-C-mannoses or by non-mannosylated tryptophans. Blue bars correspond to C-mannoses in $^1C_4$ conformation. In case of C-mannosylated tryptophans, both tryptophan and mannose residues were included into calculations.

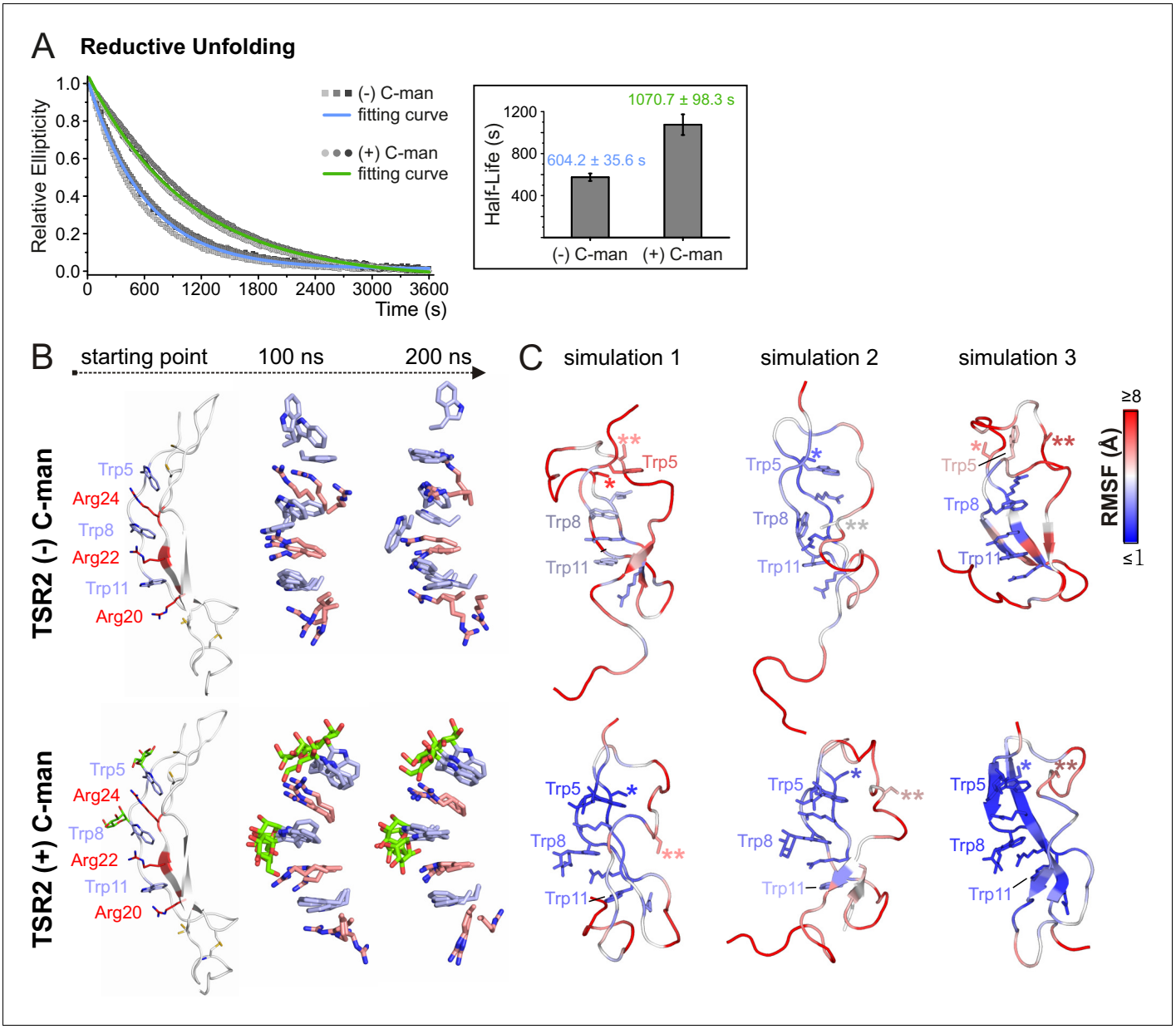

Figure 5. C-mannosylation decreases the unfolding rate of UNC-5 TSR2 during reductive denaturation. (**A**) Reductive denaturation of non-mannosylated (blue) and C-mannosylated (green) UNC-5 TSR2 monitored using CD spectroscopy at a wavelength of 229 and 228 nm, respectively. Measurements of three non-mannosylated (gray-shaded squares) and C-mannosylated (gray-shaded circles) UNC-5 TSR2 samples were averaged and fitted (***Figure 5—source data 1***). Average half-life values are depicted in the right plot (error bars show standard deviation). (**B**) Modeled structures of UNC-5 TSR2 lacking disulfide bridges without C-mannosylation (top) and with two C-mannoses on Trp5 and Trp8 (bottom) at the starting point of each simulation followed by aligned Trp-Arg ladder structures from three simulation replicates after 100 and 200 ns simulation time. Tryptophans are depicted in light-blue, mannoses in green and arginines in salmon. (**C**) Final structures of non- and C-mannosylated UNC-5 TSR2 after each 200 ns simulation, colored using a blue-white-red gradient according to the calculated root-mean-square fluctuation (RMSF) values (blue ≤1 Å; red ≥5 Å) (***Figure 5—figure supplement 1***, ***Figure 5—source data 2***). Cys26 and Cys38 residues, that are involved in the upper disulfide bridge of the TSR, are labeled with one or two asterisks, respectively.

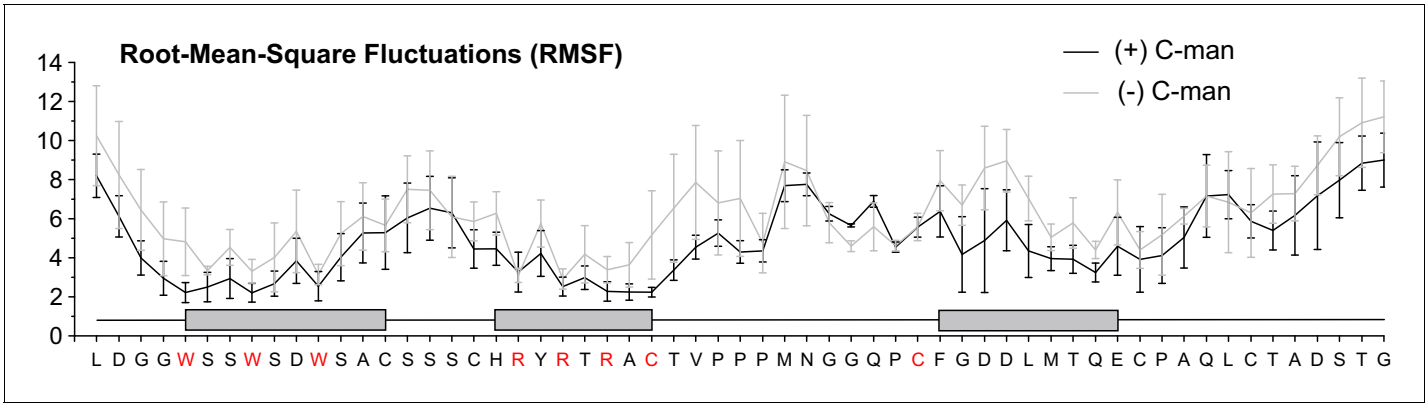

Figure 5—figure supplement 1. Side chain Root-Mean-Square Fluctuations (RMSF) of all residues from molecular dynamics simulations of the TSRs lacking disulfide bonds. Mean RMSF values from simulation triplicates are shown in black for the C-mannosylated and in gray for the non-mannosylated TSR. Error bars depict calculated standard error. The three TSR beta-strands are displayed as gray boxes above the protein sequence. Tryptophan and arginine residues forming the Trp-Arg ladder, as well as Cys26 and Cys38, are highlighted in red.

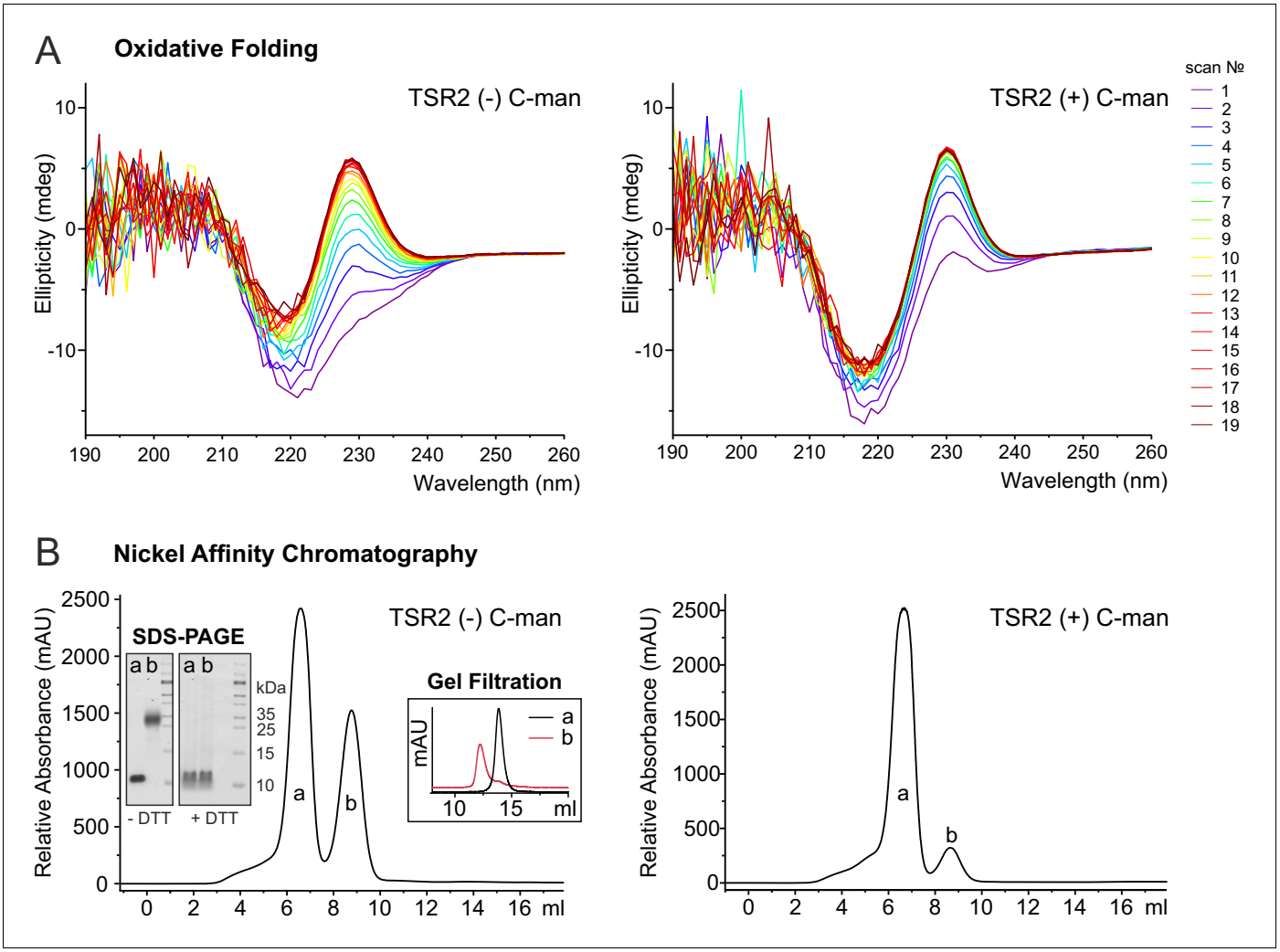

Figure 6. C-mannosylation impacts the folding of UNC-5 TSR2. (**A**) Oxidative refolding of previously reduced and unfolded non- and di-mannosylated UNC-5 TSR2 monitored by CD spectroscopy in presence of 0.5 mM GSSG and 1 mM GSH at 24°C. The first spectrum was recorded 9 min after removal of denaturating agents and addition of GSSG/GSH. Subsequent spectra were recorded every 10 min. (**B**) Nickel affinity purification chromatograms of secreted non- and C-mannosylated His-tagged TSR2 from *Drosophila* S2 cells. Whereas C-mannosylated TSR2 appeared primary as monomer (**a**), non-mannosylated TSR revealed a high amount of dimeric structures (**b**), which bound stronger to the nickel affinity column and were confirmed by gel filtration chromatography and non-reducing SDS-PAGE. Highly increased formation of dimers was consistently observed in over ten independent purifications.

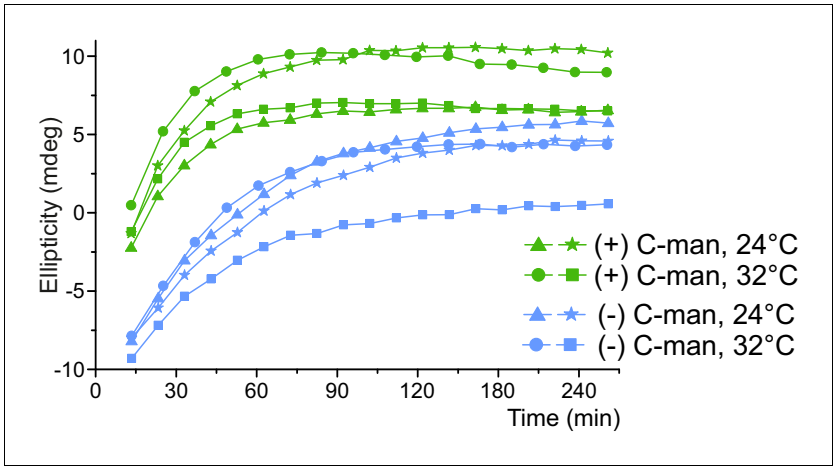

Figure 6—figure supplement 1. Time plot of the oxidative refolding presented in ***Figure 6A***. Four independent folding reactions of proteins with and without C-mannose were followed at a wavelength of 229 and 228 nm, respectively, at 24 or 32˚C.

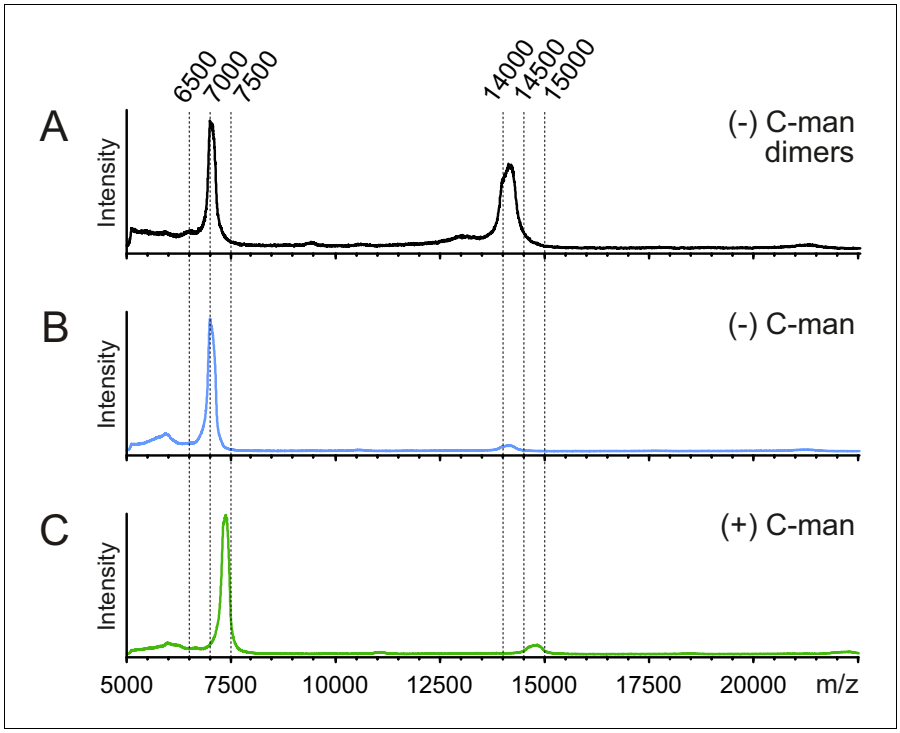

Figure 6—figure supplement 2. MALDI-TOF MS analysis of monomeric and dimeric UNC-5 TSR2 structures. Secreted non- and C-mannosylated TSR2 from *Drosophila* S2 cells were purified by nickel affinity (***Figure 6B***) and gel filtration and analyzed by MALDI-TOF MS with 5 mg/ml α-cyano-4-hydroxycinnamic acid as matrix, using a 5800 MALDI TOF/TOF (ABSciex). (**A**) The nickel affinity chromatography fraction b (***Figure 6B***, left panel) was detected at two m/z values. One peak corresponds to the expected mass of a singly charged dimer of TSR2 (monoisotopic m/z: 14284.88). A second peak likely represents the doubly charged dimer of TSR2 (calculated m/z: 7142.94). (**B**) The nickel affinity chromatography fraction a (***Figure 6B***, left panel) was mainly detected at a size corresponding to the calculated monomer (m/z: 7142.94). (**C**) The nickel affinity chromatography fraction a (***Figure 6B***, right panel) likely represents the expected singly charged monomer with two mannoses attached (calculated m/z: 7467.04).

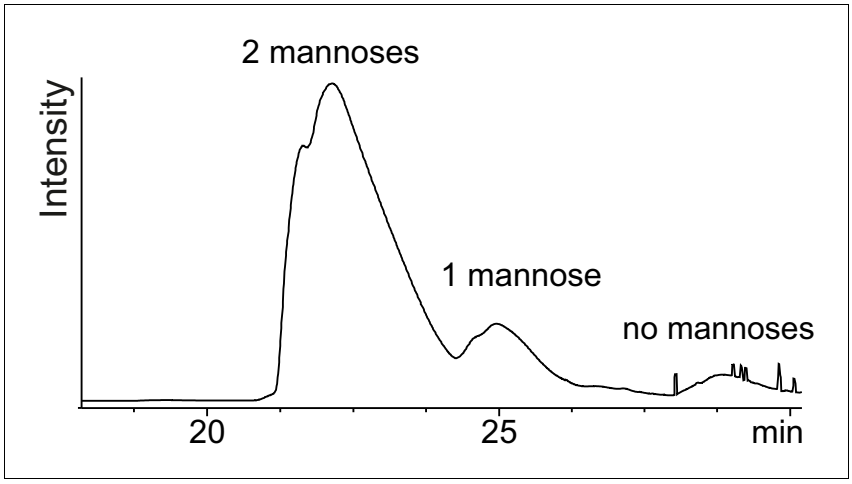

Figure 6—figure supplement 3. Separation of di-, mono- and non-mannosylated UNC-5 TSR2 by C18 chromatography. UNC-5 TSR2 from stably transfected S2 cells + DPY-19 after purification by nickel affinity chromatography was applied to the Xbridge Prep C_{18}5 µm, 10 × 50 mm column (Waters), equilibrated in 10% acetonitrile, 0.05% trifluoroacetic acid at 1 ml/min. Di-, mono- and non-mannosylated TSR2 were eluted with a linear gradient of 10–40% acetonitrile over 30 ml and detected at 280 nm.